Journal of Energy and Power Engineering 18 (2024) 93-103
doi: 10.17265/1934-8975/2024.03.003

Integration of a Fault-Tolerant H-Bridge Inverter into the Photovoltaic System for DC-AC Conversion of Electrical Energy

Dobsoumna Emmanuel[1], Djondin é Philippe[1,2], Issa Dieudonn é[1], Douniya Edouard[1] and Ronw é Djorw é Fr éd éric[1]

1. Department of Physics, Faculty of Sciences, The University of Ngaound é r é, P.O. Box 454, Ngaound é r é, Cameroon

2. Department of Physics, Higher Teacher Training College of Bertoua, The University of Bertoua, P.O. Box 652, Bertoua, Cameroon

Abstract: The photovoltaic system is experiencing great growth in the production of electrical energy these days. It plays a vital role in the production of electrical energy in isolated towns. It is generally either stand-alone or connected to a network. The energy produced by the photovoltaic generator is in continuous form; the conversion from its continuous form to the alternating form requires a converter: the inverter. In order to improve the quality of the waveform, we moved from the classic solar inverter to multilevel inverters. These multilevel inverters are equipped with power switches which are required to withstand strong fluctuations in the voltage produced by the GPV (photovoltaic generator). It is obvious that the degradation of the inverter leads to a distortion of the wave quality. This article presents the simulation of the GPV-Chopper Boost-Inverter chain in fault-tolerant cascaded H-bridges in order to overcome the difficulties of voltage constraints experienced by power switches (IGBT: insulated gate bipolar transistor). The results of simulations carried out in Matlab/Simulink show good performance of the designed inverter model.

Key words: Photovoltaic generator, boost chopper, fault-tolerant, H-bridge inverter, GPV-chopper.

Nomenclature

I_{sc}	Short circuit current
K_i	Short circuit current of the entire system at 25 ℃ and 1,000 W/m^2
T	Operating temperature
Tn	Rated temperature
G	Solar irradiation
Q	Electron charge (1.6 × 10^{-19} C)
V_{oc}	Open circuit voltage
N	Ideality factor
K	Boltzmann constant (1.38 × 10^{-23} J/K)
E_{g0}	Band gap energy of semiconductor
N_S	Number of photovoltaic cells connected in series
N_P	Number of photovoltaic modules connected in parallel
R_S	Series resistance
R_{sh}	Shunt resistance
Vt	Diode thermal voltage

Corresponding author: Djondin é Philippe, Ph.D, associate professor, research fields: photovoltaic cells and renewable energy.

1. Introduction

The strong growth in the use of photovoltaic modules has and continues to arouse the curiosity of researchers, which has led to major technological innovations and falling costs not only in the field of solar energy but also in power electronics. In order to improve the profitability of solar systems, we used the boost converter, which has the role of increasing the value of the voltage of the photovoltaic DC (direct current) bus, and stabilizing the fluctuations caused by the variation of the solar irradiation and temperature [1, 2]. In order to improve the wave quality during the conversion from the DC form to the AC (alternating current) form of electrical energy, we have moved from the use of photovoltaic microinverters to multilevel inverters. It should be noted that multilevel inverters have brought an undeniable benefit to

photovoltaic systems [3, 4]. Furthermore, these multilevel inverters are equipped with power switches (IGBT) which are subject to significant voltage constraints. In addition, the photovoltaic generator has a non-linear characteristic in terms of power produced as a function of illumination and temperature, which can consequently damage power switches such as IGBTs which are designed to withstand low and medium voltages [3, 5]. In this paper, we will present in Section 2 the overall structure of the study model, after which, we will proceed by presenting in Section 3 the real characteristic of a photovoltaic cell; in Section 4 the structure of the boost converter; a fault-tolerant H-bridge inverter model will be presented in Section 5, and Section in 6 we will present the simulation results of the GPV-Chopper Boost-Inverter chain in fault-tolerant cascaded H-bridges. The inverter control technique used is that of triangular-sinusoidal pulse width modulation with a phase arrangement of the carriers.

2. Materials and Methods

2.1 Materials

The photovoltaic conversion chain that we are going to study is made up of a photovoltaic module responsible for converting incident energy from the sun (photon) into electrical energy in continuous form, a DC-DC converter or boost chopper responsible for increasing the value of the voltage produced by the PV module, the accumulator batteries responsible for storing energy at the boost output and the famous tolerant cascaded H-bridge inverter ensuring the DC-AC conversion and maintaining continuity of operation (Fig. 1).

2.1.1 Photovoltaic Generator

A photovoltaic generator is an assembly of photovoltaic modules. A photovoltaic module/panel is the series/parallel association of photovoltaic cells according to the voltage/current requirement. The photovoltaic cell is the fundamental element in the conversion of solar rays (photons) into electricity. The equivalent electrical circuit of the photovoltaic cell is shown in Fig. 2.

The mathematical model that governs the diagram in Fig. 2 is represented by the equation:

$$I_{PV} = I_{ph} - I_d - I_{sh} \quad (1)$$

Now the current in the diode is known and is expressed by:

$$I_d = I_0 \left[exp\left(\frac{q * (V + I * R_S)}{n * K * N_s * T} \right) - 1 \right] \quad (2)$$

With I_0, the saturation current:

$$I_0 = I_{rs} * \left[\frac{T}{Tn} \right] * exp\left[\frac{q * E_{g0} * \left(\frac{1}{T_n} - \frac{1}{T} \right)}{n * K} \right] \quad (3)$$

I_{rs}, reverse saturation current:

$$I_{rs} = \frac{I_{sc}}{exp\left[q * \frac{V_{0c}}{n * K * N_s * T} \right]} \quad (4)$$

The current through the shunt resistor is given by:

$$I_{sh} = \frac{V + I + R_s}{R_{sh}} \quad (5)$$

The current of the incident photon is given by:

$$I_{ph} = [I_{sc} + K_i * (T - 298)] * \frac{G}{1000} \quad (6)$$

Hence finally the current produced by the cell is:

$$I_{pv} = P_{ph} - I_0 * \left[exp\left(\frac{q * (V + I + R_s)}{n * K * N_s * T} \right) - 1 \right] - I_{sh} \quad (7)$$

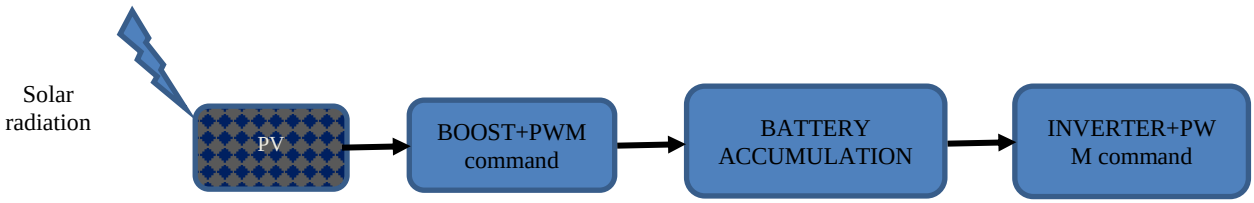

Fig. 1 DC-AC conversion algorithm.

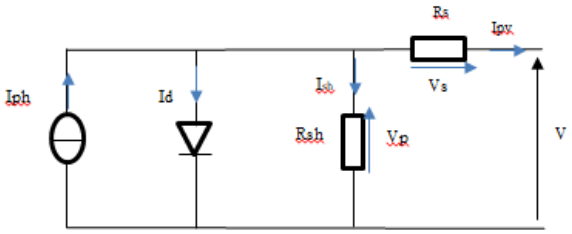

Fig. 2 Equivalent electrical circuit of a photovoltaic cell.

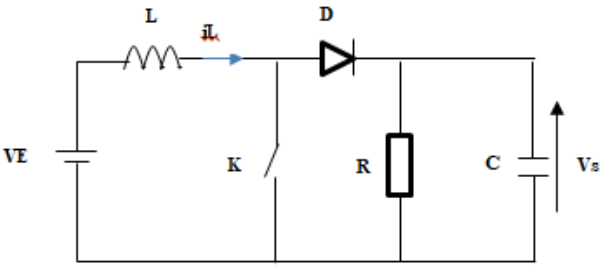

Fig. 3 Equivalent electrical circuit of a boost converter.

2.1.2 Boost Chopper

Fig. 3 represents the electrical circuit of a voltage boost converter commonly called boost. Assuming that this system operates in continuous mode, we can describe it in the following:

(1) step 1: $0 < t < \omega T$

Switch K is closed, diode D is blocked; we have:

$$V_E = L\frac{d(i_L)}{dt} \Rightarrow i_L(t) = I_m + \frac{V_E}{L}t \tag{8}$$

At time $t = \omega T$, the current in the inductor reaches the peak value:

$$I_M = I_m + \frac{V_E}{L}\omega T \tag{9}$$

(2) step 2: $\omega T < t < T$

At $t = \omega T$, we open the switch K; diode D conducts; So we have:

$$V_E - V_S = L\frac{d(i_L)}{dt} \Rightarrow i_L(t) = I_M - \frac{V_S - V_E}{L}(t - \omega T) \tag{10}$$

At time $t = T$, the current in the inductor reaches its minimum value:

$$I_m = I_M - \frac{V_S - V_E}{L}(1 - \omega)T \tag{11}$$

Let $d(i_L)$ be the ripple of the current in the inductance defined by:

$$d(i_L) = I_M - I_m \tag{12}$$

Eq. (9):

$$\Rightarrow d(i_L) = I_M - I_m = \frac{V_E}{L}\omega T \tag{13}$$

And Eq. (11) →

$$d(i_L) = I_M - I_m = \frac{V_S - V_E}{L}(1 - \omega)T \tag{14}$$

By combining Eqs. (13) and (14), we obtain the voltage at the converter output:

$$V_S = \frac{V_E}{1 - \omega} \tag{15}$$

We see that the value of the output voltage only depends on the value of the input voltage and the duty cycle ω; with $\omega \in [0, 1]$ in the literature.

2.1.3 Fault-Tolerant H-Bridge Inverter

Table 1 below gives the operating principle of a full H-bridge inverter in healthy operating mode.

In order to improve profitability when converting electrical energy from its DC form to its AC form in photovoltaic systems, we have considered the integration of multilevel inverters in the latter. In Ref. [6], the authors proposed the integration of an asymmetric multilevel inverter with two full bridges for low voltage applications. In Ref. [7], the authors prove the effectiveness of multilevel inverters powered by the solar photovoltaic system in the parallel active filter.

It should therefore be noted that multilevel inverters have brought an undeniable plus to photovoltaic solar systems for the conversion from DC to AC form of electrical energy. Furthermore, it is no doubt that these multilevel inverters are equipped with power switches, which are called upon to withstand stresses caused by strong variations in the DC bus voltage of the photovoltaic generator. In order to overcome this problem, the authors in Ref. [8], propose a system that includes a microgrid for energy production and storage (wind turbine, photovoltaic panels and batteries) and load elements (heat pump) which consume electrical energy to provide thermal heating of buildings. In Ref. [9], the authors propose the integration of chemical storage batteries with an H-bridge inverter. The authors in Ref. [10],

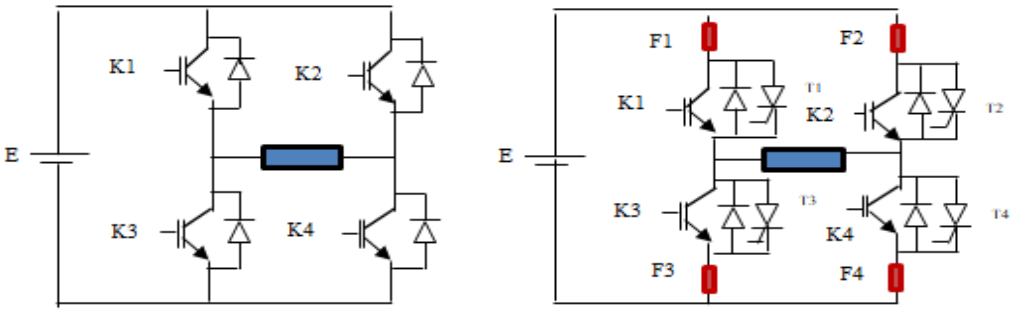

(a) (b)

Fig. 4 Classic model on the left and tolerant model on the right of the full H-bridge inverter.

Table 1 Possible switching states of an H-bridge inverter.

K1	K2	K3	K4	Output voltage
1	0	0	1	E
1	1	0	0	0
0	0	1	1	0
0	1	1	0	-E

propose the addition of an additional arm to a three-phase inverter and the authors in Ref. [11] propose the addition of a 4th additional arm of FC (flying capacitor) type to a three-phase NPC (neutral-point clamped) inverter. In this paper, we propose to mount a thyristor in parallel with each IGBT (i.e. antiparallel with each diode), and a fuse at each input of each phase of a full H-bridge inverter as shown in Fig. 4. In the presence of a fault on an IGBT (short circuit or open circuit), the thyristor being capable of withstanding high tensions, automatically takes over and drives. The voltage value at the inverter output remains unaffected.

2.2 Methods

In this section, we present the method we used.

- For the design of the tolerant H-bridge inverter

To design the classic H-bridge inverter, we proceeded by detecting and locating the faults; this phase consists of studying the inverter in degraded mode, and making a comparative study of the results obtained with those in healthy mode. Then we isolated the detected faults; this phase consists of the electrical isolation of the damaged semiconductors, by adding a fuse to each input of each phase. Finally, we reconfigured the post-faults; here it was sufficient to mount a thyristor in parallel with each IGBT. Since a thyristor is capable of supporting high powers, it would therefore be capable of supporting an excess voltage/current during a short circuit/open circuit that could damage an IGBT transistor.

- For the control of the fault-tolerant H-bridge inverter

Because of its simplicity and efficiency in controlling the complete H-bridge inverter, the control used here is the sine-triangle PWM (pulse-width modulation) with in-phase arrangement of the carrier signals. The main power switch and its redundant are controlled by the same signal as shown in Fig. 5.

Pulse width modulation is achieved by comparing a low-frequency modulated wave (reference voltage) with a high-frequency triangular-shaped carrier wave. The switching times are determined by the intersection points between the carrier and the modulator, the switching frequency of the switches is set by the carrier. In three-phase, three sinusoidal references phase-shifted by (2pi/3) at the same frequency *f*. As at the inverter output, the voltage is not purely sinusoidal, so it includes harmonics, which are the only ones responsible for the interference, which generates additional losses. This PWM is used to remedy these problems and has the following advantages [12]:

(1) Variation of the output voltage frequency;

(2) Elimination of certain voltage harmonics.

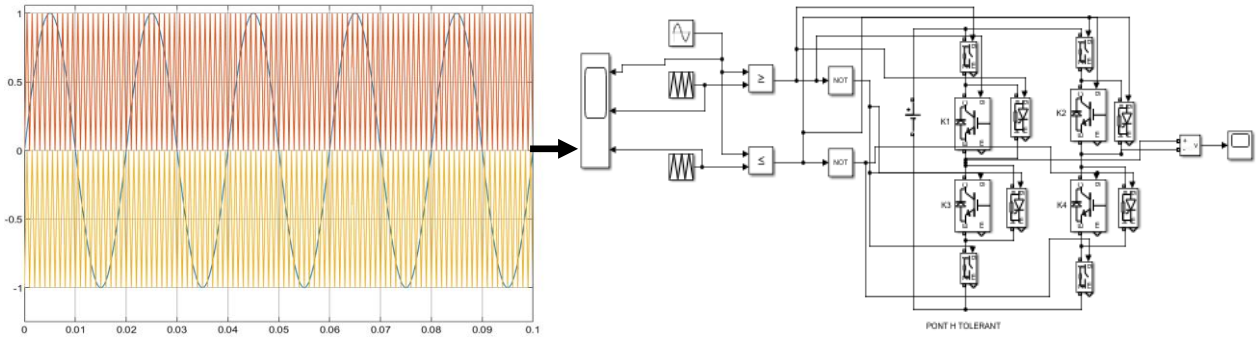

Fig. 5 Triangular-sinusoidal PWM control technique of a fault-tolerant H-bridge inverter.

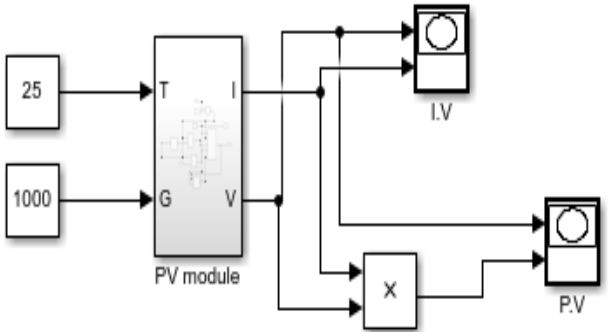

Fig. 6 Simulink block of a photovoltaic module.

- For GPV simulation

Here, we used mathematical logic connectors in Matlab/Simulink (Fig. 6) to simulate the resulting equations of the photovoltaic module:

Saturation current:

$$I_0 = I_{rs} * \left[\frac{T}{Tn}\right] * exp\left[\frac{q * E_{g0} * \left(\frac{1}{T_n} - \frac{1}{T}\right)}{n * K}\right]$$

Reverse saturation current:

$$I_{rs} = \frac{I_{cc}}{exp\left[q * \frac{V_{c0}}{n * K * N_s * T}\right] - 1}$$

The current through the shunt resistor:

$$I_{sh} = \frac{V + I + R_s}{R_{sh}}$$

The current of the incident photon:

$$I_{ph} = [I_{cc} + K_i * (T - 298)] * \frac{G}{1000}$$

The current produced by the cell:

$$I_{PV} = I_{ph} - I_d - I_{sh}$$

or

$$I_d = I_0 \left[exp\left(\frac{q * (V + I * R_S)}{n * K * N_s * T}\right) - 1\right]$$

Hence

$$I_{pv} = P_{ph} - I_0 * \left[exp\left(\frac{q * (V + I + R_s)}{n * K * N_s * T}\right) - 1\right] - I_{sh}$$

The overall GPV-BOOST-Bridge H circuit looks like below (Fig. 7).

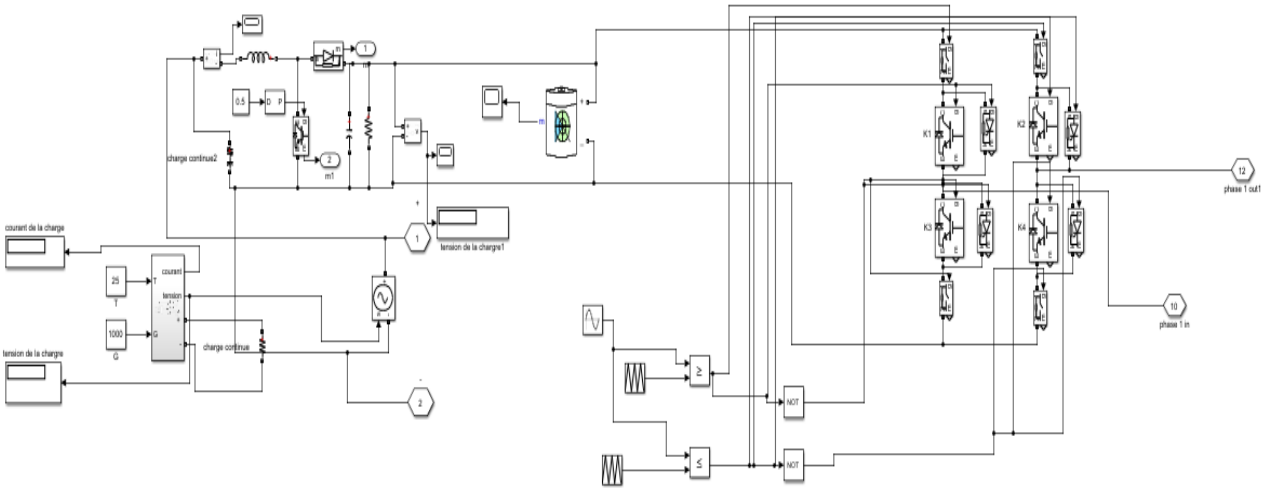

Fig. 7 Simulink block of the fault-tolerant GPV-boost-H-bridge inverter system.

3. Simulation Results

The current-voltage characteristic of the PV module shows that the current evolves while keeping its constant (despite small fluctuations) and begins to fall at a certain point until it cancels out at the value of the open circuit voltage (V_{oc}). Table 2 presents simulation parameters of the PV.

The current-voltage characteristic of the PV module shows (Fig. 8) that the power changes considerably with the voltage until reaching a threshold from which it begins to fall and disappears at the value of the open circuit voltage. This point where the power value is maximum is called the point of maximum power (P_{max}) with coordinates (I_{mp}, V_{mp}) determined by the tangent method.

Fig. 9a shows the voltage at the output of the boost converter. This voltage changes considerably with the duty cycle. It takes a little time to grow and then maintains its consistency despite small fluctuations [13, 14].

Fig. 9b represents the behavior of the storage battery during operation; at the beginning it is full, and begins to discharge considerably over time.

Fig. 10 represents the carrier signals and the reference signal for controlling an inverter with 5 full bridges mounted in cascade, i.e. 11 voltage levels. The reference signal is a sinusoid; it represents the characteristic of the signal expected at the output of the inverter. The carrier signals are triangular; they ensure the switching rate of the inverter power switches. For sine-triangle PWM control, the number of carriers is twice the number of bridges. So in our case, we have 10 carrier signals.

Fig. 11 represents the output voltage of the 5 full bridge inverters in healthy operating mode. A value of 1,183 V is recorded with a total harmonic distortion by 8.08% [7].

Fig. 12 represents the output voltage of the 5 full bridge inverters in degraded operating mode (with the 1st switch of the 1st bridge (K1) held open) whose value dropped from 1,183 V to 1,154 V with a total harmonic distortion of 8.08% [Figs. 13, 14]. We therefore record a deterioration in the voltage level in the presence of a fault. The same study is carried out on switches K2, K3, K4; the couple (K1K4) responsible for generating the voltage of value *E*; the couple (K2K3) responsible for generating the voltage of value -*E*; the couples (K1K2), (K3K4) responsible for generating the voltage of value 0; the 2 pairs (K1K3), (K2K4) made up of a main switch and its complementary, as well as the 4 switches of an H bridge simultaneously; and the results are mentioned in Table 3.

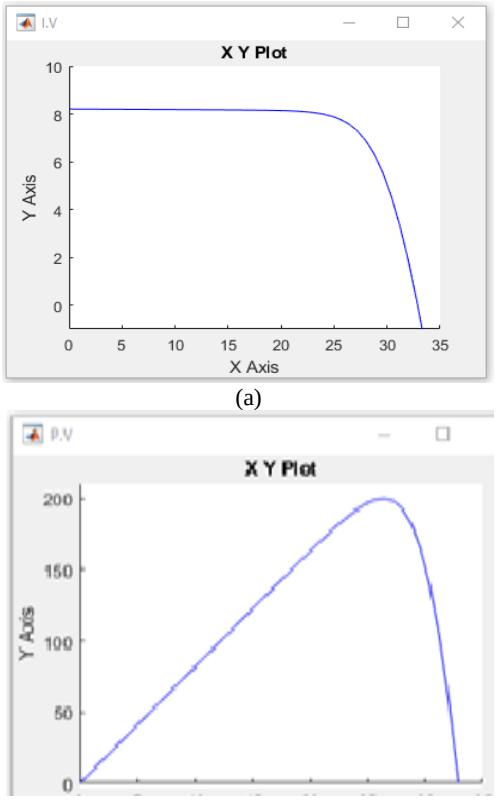

(a)

(b)

Fig. 8 Behavior of current (a) and power (b) at the GPV output as a function of voltage: case where irradiation = 1,000 W/m^2 and temperature = 25 ℃.

Table 2 Evaluation of the PV module in Simulink (for N_s = 54, N_p = 1) and simulation parameters.

Parameters	Values
Maximum power of a PV module	200 W
Maximum power voltage V_{mp}	26.4 V
Maximum power current I_{mp}	7.58 A
Open circuit voltage V_{co}	32.9 V
Short circuit current I_{sc}	8.21 A
Number of cells in series N_s	54
Number of cells in parallel N_p	1
Boost output voltage V_s	237.2 V

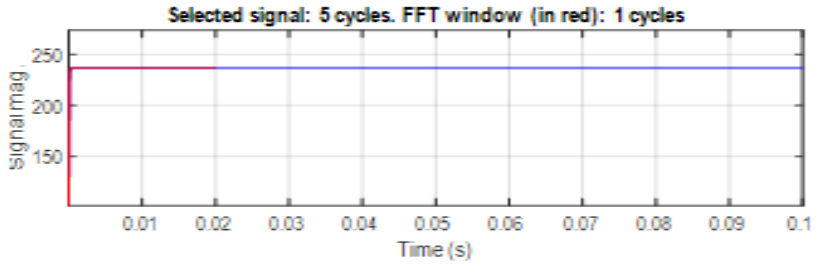

(a)

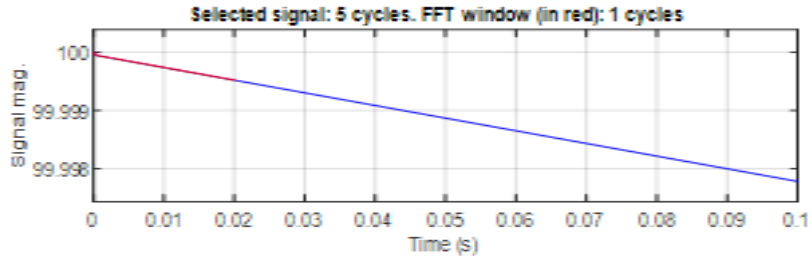

(b)

Fig. 9 Voltage at the output of the boost converter (a) and in the battery (b).

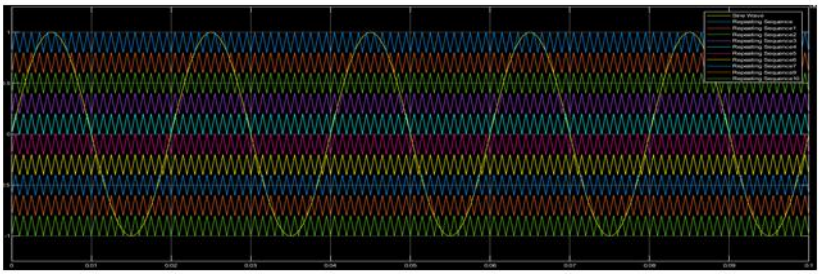

Fig. 10 Behavior of the carrier signals and the reference.

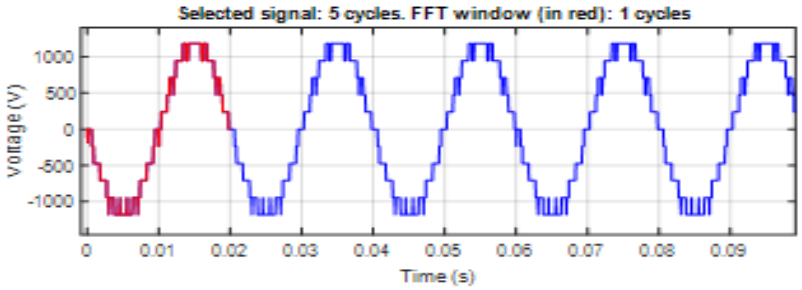

(a)

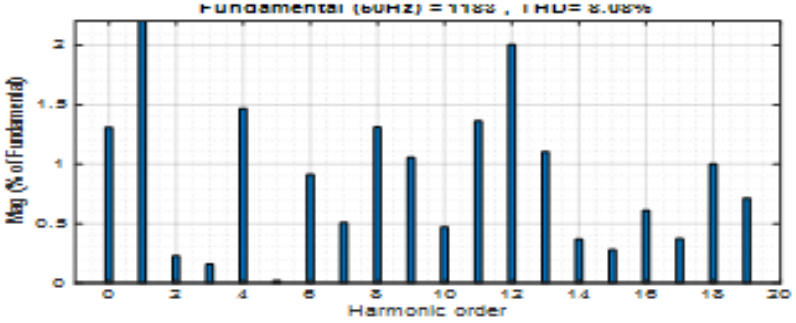

(b)

Fig. 11 Classic 5 H-bridge inverter voltage (11 levels) powered by GPV/total harmonic distortion.

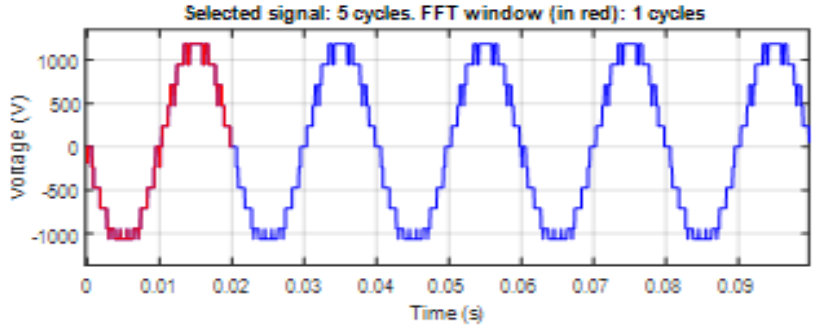

(a)

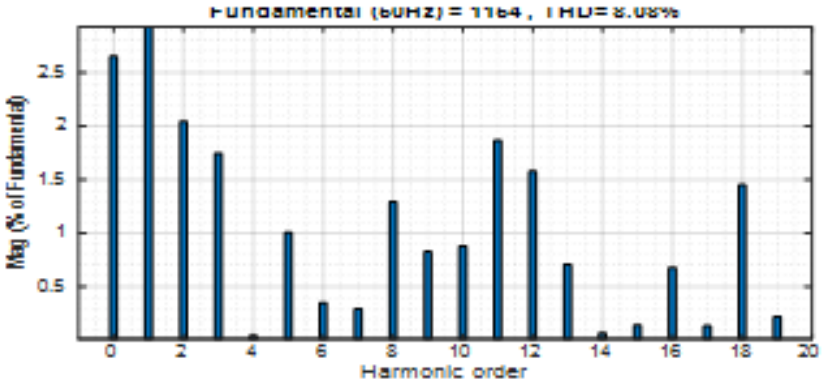

(b)

Fig. 12 Appearance of the inverter voltage at 5 classic H-bridges (11 levels) supplied by a GPV with the 1st switch of the 1st bridge K1 kept open/total harmonic distortion.

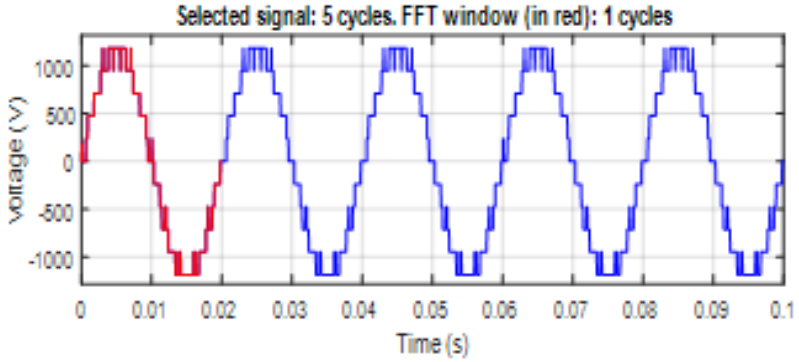

(a)

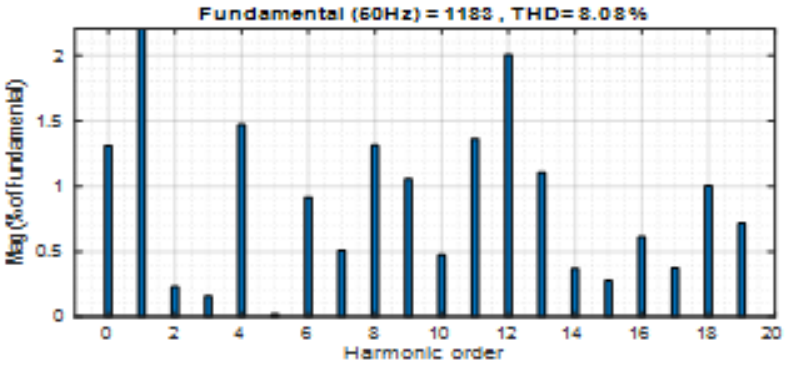

(b)

Fig. 13 Shape of the inverter voltage with 5 tolerant H-bridges (11 levels) powered by a GPV /total harmonic distortion.

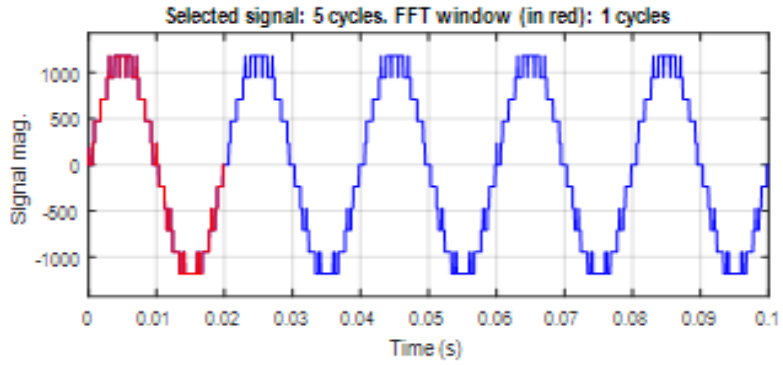

(a)

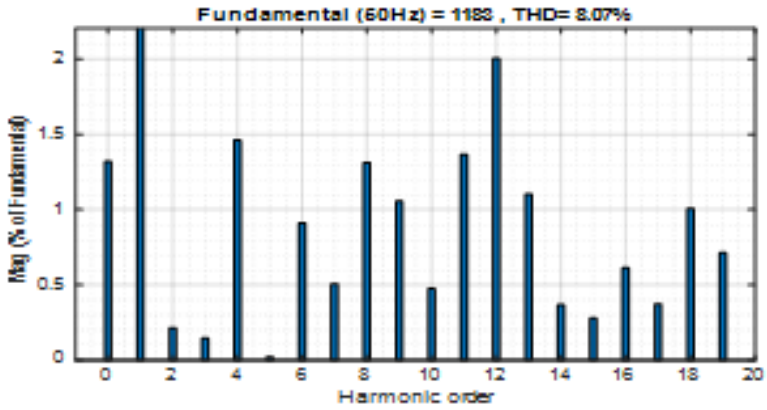

(b)

Fig. 14 Shape of the inverter voltage at 5 tolerant H-bridges (11 levels) supplied by a GPV with the 1st switch of the 1st bridge (K1) kept open/total harmonic distortion.

Table 3 Summary of the voltage values and harmonic distortion rates of the two inverter models in degraded operating mode.

	Switch(es) held open		0	K1	K2	K3	K4
Model	Classic	Voltage (V)	1,183	1,154	1,133	1,154	1,133
		THD (%)	8.08	8.08	9.02	8.04	9.07
	Tolerant	Voltage (V)	1,183	1,183	1,183	1,183	1,183
		THD (%)	8.08	8.07	8.08	8.07	8.08

K1K4	K2K3	K1K2	K3K4	K1K3	K2K4	K1K2 K3K4	K1K4
1,104	1,104	1,104	1,104	1,125	1,083	1,025	1,104
10.22	10.13	10.17	10.17	9.72	11.87	16.80	10.22
1,183	1,183	1,183	1,183	1,183	1,183	1,182	1,183
8.07	8.07	8.07	8.07	8.07	8.08	8.06	8.07

We then continue to keep switches K2, K3, K4 open; the couple (K1K4) responsible for generating the voltage of value *E*; the couple (K2K3) responsible for generating the voltage of value -*E*; the couples (K1K2), (K3K4) responsible for generating the voltage of value 0; the 2 pairs (K1K3), (K2K4) made up of a main switch and its complementary, as well as the 4 switches of an H-bridge simultaneously.

We see that for the classic model the value of the voltage and the total harmonic distortion deteriorate in the presence of a fault; and the degradation rate is a function of the size of the defect. In the case of the tolerant model, we see that the value of the voltage and the distortion rate remain unchanged in degraded mode as in healthy mode.

4. Conclusion

DC-AC power conversion has become a more widespread activity in the field of electrical energy production and consumption. The problem of stability of converters in this field (inverters) arouses more curiosity among researchers nowadays. It is indeed true that the integration of multilevel inverters in photovoltaic applications has made an undeniable plus. The simulation results presented in this paper also show that the designed fault-tolerant H-bridge inverter model improves the availability and continuous service conditions of this conversion system. And as a perspective to this work, we recommend connecting the designed system to the parallel active filter.

Acknowledgements

The authors would like to thank the journal editor and all organizations that provided data for this research.

References

[1] Sameera, Tariq, M., and Rihan, M. 2024. "Analysis of the Impact of Irradiance, Temperature and Tilt Angle on the Performance of Grid-Connected Solar Power Plant." *Measurement: Energy* 2: 100007. doi.org/10.1016/j.meaene.2024.100007.

[2] Achim, W., Vu, V. T., Ronnie, B., and Johan, N. 2006. "Voltage Fluctuations on Distribution Level Introduced by Photovoltaic Systems." *IEEE Transactions on Energy Conversion* 21 (1): 202-9. doi: 10.1109/TEC.2005.845454.

[3] Khan, M., Raza, M. A., Jumani, T. A., Mirsaeidi, S., Ali, A., Abbas, G., Touti, E., and Alshahir, A. 2023. "Modeling of Intelligent Controllers for Solar Photovoltaic System under Varying Irradiation Conditions." *Front. Energy Res.* 11: 1288486. doi: 10.3389/fenrg.2023.1288486.

[4] Anssi, M., Seppo, V., and Teuvo, S. 2010. "Dynamic Terminal Characteristics of a Photovoltaic Generator." In *Proceedings of 14th International Power Electronics and Motion Control Conference EPE-PEMC 2010*, 6-8 September 2010, Ohrid, Macedonia. doi: 10.1109/EPEPEMC.2010.5606786.

[5] Lee, J. H., and Lee, K. B. 2017. "A Fault Detection Method and a Tolerance Control in a Single-Phase Cascaded H-Bridge Multilevel Inverter." *IFAC-Papers Online* 50 (1): 7819-23. doi: 10.1016/j.ifacol.2017.08.1058.

[6] Mudadla, D., Sandeep, N., and Rao, G. R. 2015. "Novel Asymmetrical Multilevel Inverter Topology with Reduced Number of Switches for Photovoltaic Applications." In *Proceedings of the 2015 International Conference on Computation of Power, Energy, Information and Communication (ICCPEIC)*, 22-23 April 2015, Melmaruvathur, India, pp. 123-8. doi: 10.1109/ICCPEIC.2015.7259452.

[7] Kamel, S., and Ameen, M. 2021. "A Fault-Tolerant Photovoltaic Integrated Shunt Active Power Filter with a 27-Level Inverter." *International Journal of Electrical and Computer Engineering* 11 (2): 1166-77. ISSN: 2088-8708, doi: 10.11591/ijece.v11i2.pp1166-1177.

[8] Salman, A., Williams, A., Amjad, H., Kamran Liaqat Bhatti, M., and Saad, M. 2015. "Simplified Modeling of a PV Panel by Using PSIM and Its Comparison with Laboratory Test Results." In *Proceedings of the Conference: IEEE GHTC 2015*, October 8-11, 2015, Seattle, WA, USA, pp. 360-6. doi: 10.1109/GHTC.2015.7343997.

[9] Taghizadeh, H., and Tarafdar Hagh, M. 2010. "Harmonic Elimination of Cascade Multilevel Inverters with Nonequal DC Sources Using Particle Swarm Optimization." *IEEE Trans. Ind. Electron* 57 (11): 3678-84. doi: 10.1109/TIE.2010.2041736.

[10] Quanyou, P., Hongchen, L., Pat, W., and Fengjiang, W. 2019. "High Step-Up Cascaded DC-DC Converter Integrating Coupled Inductor and Passive Snubber." *IET Power Electronics* 12: 2414-23. https://doi.org/10.1049/iet-pel.2018.5706.

[11] Lezana, P., Pou, J., Meynard, T. A., Rodriguez, J., Ceballos, S., and Richardeau, F. 2010. "Survey on Fault Operation on Multilevel Inverters." *IEEE Transactions on Industrial Electronics* 57 (7): 2207-18. doi: 10.1109/TIE.2009.2032194.

[12] Rajesh, J., Jayaram, N., Satya, V., and Kishore, P. 2022. "Grid Integration of Three Phase Solar Powered Fault-Tolerant Cascaded H-Bridge Inverter." *International Journal of Circuit Theory and Applications* 50 (7): 2566-83. doi.org/10.1002/cta.3272.

[13] Sim, H. W., Lee, J. S., and Lee, K. B. 2014. "A Detection Method for an Open-Switch Fault in Cascaded H-Bridge Multilevel Inverters." In *Proceedings of the 2014 IEEE Energy Conversion Congress and Exposition (ECCE)*, 14-18 September 2014, Pittsburgh, PA, USA, pp. 2101-6. doi: 10.1109/ECCE.2014.6953680.

[14] Senbakaraj, K. B., Senbakaraj, Periyasamy, and Poongkabilan, 2020. "THD Reduction in Multi-level Inverters Based on Multicarrier Pulse Width Modulation Technique." *Int. J. Eng. Adv. Technol.* 9 (4): 1970-7. doi: 10.35940/ijeat.d8994.049420.

[15] Hamza, H., Song-Manguelle, J. J., Lingom, P. M., Nyobe-

Yome, J. M., and Doumbia, M. L. 2023. "A Review of Fault-Tolerant Control Methods for Cascaded H-Bridge Multilevel Inverters." In *Proceedings of the IEEE 14th International Conference on Power Electronics and Drive Systems (PEDS)*, 7-10 August 2023, Montreal, Canada, pp. 1-7. doi: 10.1109/PEDS57185.2023.10246759.